BMHP1-Derived Self-Assembling Peptides: Hierarchically Assembled Structures with Self-Healing Propensity and Potential for Tissue Engineering Applications

Fabrizio Gelain,[†,‡,§,*] Diego Silva,[†,‡] Andrea Caprini,[†,‡] Francesca Taraballi,[†,‡] Antonino Natalello,[‡,⊥] Omar Villa,[†,‡] Ki Tae Nam,[¶,#] Ronald N. Zuckermann,[¶] Silvia Maria Doglia,[‡,⊥] and Angelo Vescovi[†,‡,§]

[†]Center for Nanomedicine and Tissue Engineering—A.O. Ospedale Niguarda Ca' Granda, Piazza dell'ospedale maggiore 3, Milan, 20162, Italy, [‡]Biotechnology and Biosciences Department, University of Milan-Bicocca, Piazza del Scienza 2, Milan, 20126, Italy, [§]IRCCS Casa Sollievo della Sofferenza, Opera di San Pio da Pietrelcina, San Giovanni Rotondo 71013, Italy, [⊥]Consorzio Nazionale Interuniversitario per le Scienze fisiche della Materia (CNISM) UdR Milan-Bicocca, Milan, 20126, Italy, [¶]Molecular Foundry, Lawrence Berkeley National Laboratory, 1 Cyclotron Road, Berkeley, California 94720, United States, and [#]Department of Materials Science and Engineering, Seoul National University, Gwanak-gu, 151-742, Seoul, Korea

Hydrogels, mainly ascribable to soft materials, comprise synthetic and natural polymeric materials and have a wide range of applications in 3D cell culturing, drug delivery, and tissue engineering.[1−3] However, regardless of their purity or chemical tailorability, synthetic hydrogels[4−6] may pose questions of biocompatibility of the biodegradation products and host responses upon transplantation. Naturally derived polymers,[7,8] despite their advantages, can still face various challenges like inflammatory response, pathogen transfer, and purity.[9]

Research related to low-molecular-weight self-assembling peptides (SAPs), synthetic but naturally inspired, has been rapidly expanding in the recent years. Construction of self-assembling peptide hydrogels has received considerable attention due to their potential as nanostructured materials amenable to easy functionalization and capable of creating microenvironments suited for culturing cells,[10,11] triggering tissue regeneration,[12,13] and other applications beyond life-sciences.[14] SAP scaffolds are interesting candidates for tissue engineering because of their mild self-assembling conditions and easy functionalization. They self-organize *via* formation of various noncovalent interactions in water, including hydrogen bonding, electrostatic, and $\pi-\pi$ interactions. These interactions lead to the formation of organized supramolecular assemblies that can give rise to nanofibers, nanotubes, and nanoparticles.[15,16]

ABSTRACT Self-assembling peptides (SAPs) are rapidly gaining interest as bioinspired scaffolds for cell culture and regenerative medicine applications. Bone Marrow Homing Peptide 1 (BMHP1) functional motif (PFSSTKT) was previously demonstrated to stimulate neural stem cell (NSC) viability and differentiation when linked to SAPs. We here describe a novel ensemble of SAPs, developed from the BMHP1 (BMHP1-SAPs), that spontaneously assemble into tabular fibers, twisted ribbons, tubes and hierarchical self-assembled sheets: organized structures in the nano- and microscale. Thirty-two sequences were designed and evaluated, including biotinylated and unbiotinylated sequences, as well as a hybrid peptide—peptoid sequence. *Via* X-ray diffraction (XRD), CD, and FTIR experiments we demonstrated that all of the BMHP1-SAPs share similarly organized secondary structures, that is, β-sheets and β-turns, despite their heterogeneous nanostructure morphology, scaffold stiffness, and effect over NSC differentiation and survival. Notably, we demonstrated the self-healing propensity of most of the tested BMHP1-SAPs, enlarging the set of potential applications of these novel SAPs. In *in vitro* cell culture experiments, we showed that some of these 10-mer peptides foster adhesion, differentiation, and proliferation of human NSCs. RGD-functionalized and hybrid peptide-peptoid self-assembling sequences also opened the door to BMHP1-SAP functionalization with further bioactive motifs, essential to tailor new scaffolds for specific applications. In *in vivo* experiments we verified a negligible reaction of the host nervous tissue to the injected and assembled BMHP1-SAP. This work will pave the way to the development of novel SAP sequences that may be useful for material science and regenerative medicine applications.

KEYWORDS: self-assembling peptide · self-healing scaffold · biotinylation · neural stem cell

Thanks to their biocompatibility, hydrogels like RADA16-I[17] can be utilized for regenerative medicine applications and for delivering cytokines: indeed small molecule drugs can be confined in scaffold hollow cavities and eventually interact weakly with the net surface charges of the self-assembled nanostructures thus being released slowly.[18] SAP hydrogels have been used as hemostat solutions,[19]

scaffolds for *in vitro* three-dimensional cell cultures, and *in vivo* drug delivery applications.[20] Moreover, SAPs (in the range of 2−25 residues) are easy to manufacture in large quantities (up to a few grams in case of solid-phase synthesis or 1−100 g in case of liquid-phase synthesis), that can be subsequently purified up to purities >99%. SAPs can also be modified chemically and biologically after synthesis. Such modifications may allow the construction of nanostructures promoting cell adhesion and growth,[11,21] and scaffolds promoting nervous regeneration *in vivo*.[22] Thus a new set of unprotected oligopeptides can be considered an important step toward the development of new biologically inspired biomaterials for tissue engineering and 3D cell cultures, as well as new potential tools for developing molecular switches sensitive to pH, concentration,and temperature.

Recently we showed that Bone Marrow Homing Peptide 1 (BMHP1) functional motif (PFSSTKT) can foster neural stem cell differentiation[11] and stabilize the β-sheet structures[23] found in RADA16-I nanofibers, when linked, *via* an oligo-glycine-spacer, to the RADA16-I self-assembling "core". Biotin, a water-soluble vitamin, acts as a cofactor in a number of important biochemical reactions.[24] Multiple conformational ensembles of biotin, ranging from extended to folded states, have been found in solution,[25] with the latter structures stabilized by hydrogen bonding between active groups and its carboxylic acid side chain. In this research we synthesized several variations of BMHP1 sequence to systematically explore their self-assembling propensity and biomechanical properties. We probed the characteristics of self-assembling sequences *via* atomic force microscopy (AFM), rheology tests, *in vitro* assays with human neural stem cells (hNSCs), and *in vivo* implants. BMHP1-SAP molecular structures were then analyzed *via* X-ray diffraction (XRD), circular dichroism (CD), and Fourier transform infrared (FTIR) spectroscopies, highlighting the presence of β-sheet secondary structures involved in the self-assembly phenomenon. The majority of BMHP1-SAPs were biotinylated at the N-terminus: some were showed to self-organize into tabular 10 μm-long nanofibers, others hierarchically self-assembled into complex interwoven membranes of a few micrometers width. Among them, functionalized or hybrid peptide−peptoid sequences were also tested in order to assess their potential as functionalized scaffolds for cell cultures. Interestingly, for most of the BMHP1-SAPs we also demonstrated their self-healing propensity, namely the capability of the assembled scaffolds to recover their stiffness after rupture. In this work we introduced and characterized a novel set of short SAPs featuring self-healing propensity, hierarchical self-organization, and a broad range of scaffold storage moduli; BMHP1-SAPs also exhibited a "pro-differentiative effect" over hNSCs, a negligible host reaction when injected into the spinal cord in rats. They are also amenable to further functionalizations. For all these reason BMHP1-SAPs may provide new ways of developing new self-assembling nanostructures designed for cell cultures, regenerative medicine applications, and other fields.

RESULTS AND DISCUSSION

Peptides were synthesized, purified, and characterized as described in the Experimental Methods section. Final purity was more than 95% (Supporting Information, Figure S1). Acetylated BMHP1 sequence (peptide 1: Ac-PFSSTKT-CONH$_2$) and a Gly-added version (peptide 2: Ac-GGGPFSSTKT-CONH$_2$) were tested, unsuccessfully, for their propensity in forming membranes or scaffolds when dissolved in distilled water and in phosphate-buffered saline solutions (PBS, pH 7.4).

From the literature we know that Ser and Thr residues are abundantly involved in the H-bonding network of the biotin−strepatividn complex;[26] moreover, Pro and aromatic-rich sequences[27] were demonstrated to have strong binding affinities to biotin. Thus, peptide 2, which contains Ser, Thr, Pro and Phe, was tagged with biotin at the N-terminus (peptide B3) to look for additional noncovalent interactions contributing to peptide self-assembling. B3 gave a viscous and opaque solution when dissolved in water at 3% w/v concentration and yielded a solid scaffold when exposed to PBS (1×). Consequently, we tested 28 sequence variations of peptide B3 (see Table 1, reporting numbering, peptide sequences, type of variations, and self-assembling propensity at the macroscale) and a BMHP1 randomized sequence linked to the same biotinylated triplet of glycines of peptide B3 (peptide B32). We systematically varied the sequence to explore the magnitude of the forces favoring the assembly (h-bonding, hydrophobic packing, aromatic staking, electrostatic attractions) or of those working against assembly (electrostatic repulsions).

Biotinylated peptides were named the with "B + number": the other peptides were just numbered. Ala was chosen as aliphatic approximately free of charge (at neutral pH) and poorly reactive residue to selectively test the influence of single residues over the self-assembling and bioactivity of the overall BMHP1-SAP sequences.

Specifically, sequence modifications comprise substitution of biotin with Trp (peptides 4, 5, 6, 8, 9, 20, 21, 30, 31), Gly-component length variation (peptides 1, B7, 8, 9, B25, B29), hydrophilic head truncation (peptide 5), substitution of Pro with Ala (peptides B15, B19, B24, 30, 31) or with *N*-propylglycine (peptide B28), substitution of Phe with Ala (peptide B16) or with Trp (B27), substitution of Ser with Ala (peptides B14, B24, B26, 30), peptides net charge variation *via* Ser8 substitution with Glu (B17) or replacement of Lys with positively charged

TABLE 1. BMHP1-Derived Peptide Sequence Variations

peptide identific-ation numbers	peptide sequences	biotin-ylation	substitu-tion on Lys	substitu-tions on Ser	substitu-tion on Pro	substitu-tion on Phe	Gly spacer length variation	RGD function-alization	BMHP1 random-ization	SA propen-sity[a]
1	Ac-PFSSTKT-CONH$_2$						X			NSA
2	Ac-GGGPFSSTKT-CONH2									NSA
B3	Biot-GGGPFSSTKT-CONH2	X								SA
4	Ac-WGGGPFSSTKT-CONH2									SA
5	Ac-WGGGPF-CONH$_2$									NSA
6	Ac-WGGGPFSSTLT-CONH2		X							NSA
B7	Biot-PFSSTKT-CONH$_2$	X					X			NSA
8	NH$_2$—WPFSSTKT-CONH$_2$						X			NSA
9	Ac-WPFSSTKT-CONH$_2$						X			NSA
B10	Biot-GGGPFSSTDT-CONH$_2$	X	X							ISA
B11	Biot-GGGPFSSTNT-CONH$_2$	X	X							ISA
B12	Biot-GGGPFSSTET-CONH$_2$	X	X							ISA
B13	Biot-GGGPFSSTQT-CONH$_2$	X	X							ISA
B14	Biot-GGGPFAATKT-CONH$_2$	X		X						NSA
B15	Biot-GGGAFSSTKT-CONH$_2$	X			X					SA
B16	Biot-GGGPASSTKT-CONH$_2$	X				X				NSA
B17	Biot-GGGPFSETKT-CONH$_2$	X		X						SA
B18	Biot-GGGPFSSTKTGRGD-CONH$_2$	X						X		NSA
B19	Biot-GGGAFSSTKTGRGD-CONH$_2$	X			X			X		SA
20	NH$_2$—WGGGPFSSTKTGRGD-CONH$_2$							X		NSA
21	Ac-WGGGPFSSTKTGRGD-CONH$_2$							X		NSA
B22	Biot-GGGPFSSTRT-CONH$_2$	X	X							SA
B23	Biot-GGGPFSKS-CONH$_2$	X								NSA
B24	Biot-GGGAFASTKT-CONH$_2$	X		X	X					SA
B25	Biot-GGGGGPFSSTKT-CONH$_2$	X					X			SA
B26	Biot-GGGPFASTKT-CONH$_2$	X		X						NSA
B27	Biot-GGGPWSSTKT-CONH$_2$	X				X				SA
B28	Biot-GGG(Prop)FSSTKT-CONH$_2$	X			X					SA
B29	Biot-GPFSSTKT-CONH$_2$	X					X			NSA
30	Ac-WGGGAFASTKT-CONH$_2$			X	X					SA
31	Ac-WGGGAFSSTKT-CONH$_2$				X					SA
B32	Biot-GGGKSTFPTS-CONH$_2$	X							X	NSA

[a] Identification numbers, sequences, and type of sequence variations of the tested peptides. Last column states their gelation propensity seen at the macro-scale. SA, self-assembling peptide; ISA, peptide yielding fragmented assembled scaffolds upon dissolution in water; NSA, not self-assembling peptide.

Arg (B22), oppositely charged (B10 and B12) or neutral (6, B11 and B13) residues, RGD functionalization[29] at the C-termini (peptides B18, B19, 20, and 21). Some of the proposed modifications were combined together to assess their conjoint effect.

Macroscale Characterization and Rheology. Peptide solution appearance (1% w/v) ranged from clear liquid solutions like (e.g., 4, B15, B19, B25, B28, 30) to samples getting opaque in 1—7 days after dissolution (e.g., B3, B17, B22, B24, B27, 31) as depicted in Figure 1A. Peptides B10, B11, B12, and B13 yielded macroscopically fragmented scaffolds right after dissolution in water. Some of the liquid solutions increased in viscosity over the first week after dissolution, however after 10 days no appreciable changes happened at the macroscale. Upon exposure to PBS (1×) the following peptide solutions yielded solid scaffolds as depicted in Figure 2B: B3, 4, B15, B17, B19, B22, B24, B25, B27, B28, 30, and 31. On the other hand 1, 2, 5, 6, B7, 8, 9, B14, B16, B18, 20, 21, B23, B26, B29 and B32 did not form any macroscopic structures (Table 1).

The dependence of the storage moduli (G') of the aqueous peptide solutions on concentration and time were assessed with a cone-and-plate rheometer (see methods for details) for B3 (Figure 1C). As an example, mean G' values of 3% (w/v) B3 solutions, increased from the day of dissolution (day 0) and reached a plateau at day 2 while, in case of 2% solutions, they significantly surged between day 2 and day 5. For standard rheology characterization tests G' and G'' (loss moduli) were measured by dissolving the peptides at 3% (w/v) the day before testing, and then further diluting to 1% w/v immediately prior to measurements (unless otherwise specified). At first, measurements were made of aqueous solutions, then PBS was added onto the lower plate to trigger scaffold formation, and new tests were performed. When necessary (e.g., too viscous solutions for reliable user handling or yielding a poor scaffold gelation), we lowered (B3, B22, and B24) or increased (B19, B28, 30, and 31) the peptide concentration, or waited up to
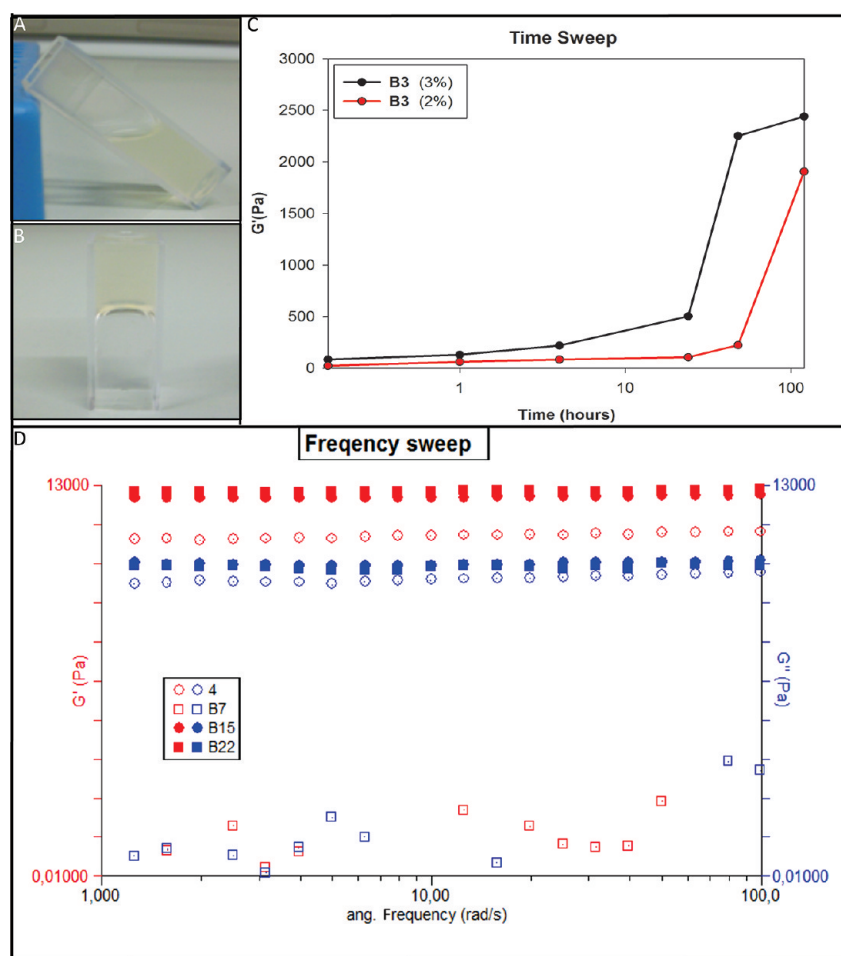
Figure 1. Rheological characterization of BMHP1-SAPs. Gelation experiment of self-assembling peptides after dissolution in distilled water (A) and subsequent addition and depletion of PBS (B). B3 solution G' kinetic dependency on peptide concentration (C): storage modulus (G') of peptide B3 dissolved at 3% (w/v) concentration reached a plateau after 2 days (variation of 7% between day 2 and day 5), while G' increased 10 times in the case of the 2% solution. (D) Storage (G') and loss (G'') moduli measurements of assembled scaffolds (peptides 4, B15, B22) or of liquid solution (peptide B7) after pH shift.

1 week (4, B27, and 30) before triggering scaffold formation with PBS.

After having added PBS, very low and nonlinear G' and G'' values were detected for all of the peptides not giving solid scaffolds at the macroscale (e.g., peptide B7 in Figure 1D): similar results were obtained for the same peptides dissolved at concentrations ranging from 0.5% to 10% (w/v) and up to 10 days after dissolution in water. A stable linear frequency response was detected for all the other peptides, with G' values (representing the elastic character of the materials) well above G'' values (representing the viscous character of the materials), resembling the typical responses of solid structures[30] (see Figure 1D). Because B10, B11, B12, and B13 immediately self-assembled upon dissolution, sample preparation and transfer resulted in aqueous solutions of fragmented scaffolds, thus measurements were not reported.

A lack of positively charged residues likely caused B10, B11, B12, and B13 to self-assemble immediately upon dissolution, thus preventing their usage as jellifying aqueous solutions for cell scaffolding purposes or

as injectable biomaterials for *in vivo* applications. Indeed we can infer that electrostatic repulsions given by positively charged residues (mainly Lys) of the other sequences may prevent the formation of solid scaffolds in the short term, but, on the other hand, they are screened by ionic charges, thus speeding up their self-assembly in neutral pH buffers.

In all of the BMHP1-SAPs the G' value differences measured before and after PBS addition spanned from 2 to 4 orders of magnitude (Supporting Information, Table S1). Among the peptides giving soft scaffold (100−1000 Pa range) we include peptides 4, B19, B25, B28, and 30. On the opposite side, SAPs yielding solid stiff scaffolds are B15, B22, B24, B27, and 31 (5000−9000 Pa range).

In the case of B15 the Ala substitution of Pro did produce a stiff solid scaffold ($G' = 8500$ Pa), while for B24 the replacement of Pro and Ser8 with alanines brought the overall scaffold stiffness to values higher ($G' = 6502$ Pa) than peptide B3 ($G' = 2917$ Pa). Gly-spacer variations, apart from B25, prevented the tested peptide from forming any scaffolds (B7, 8, 9, B29). Biotin
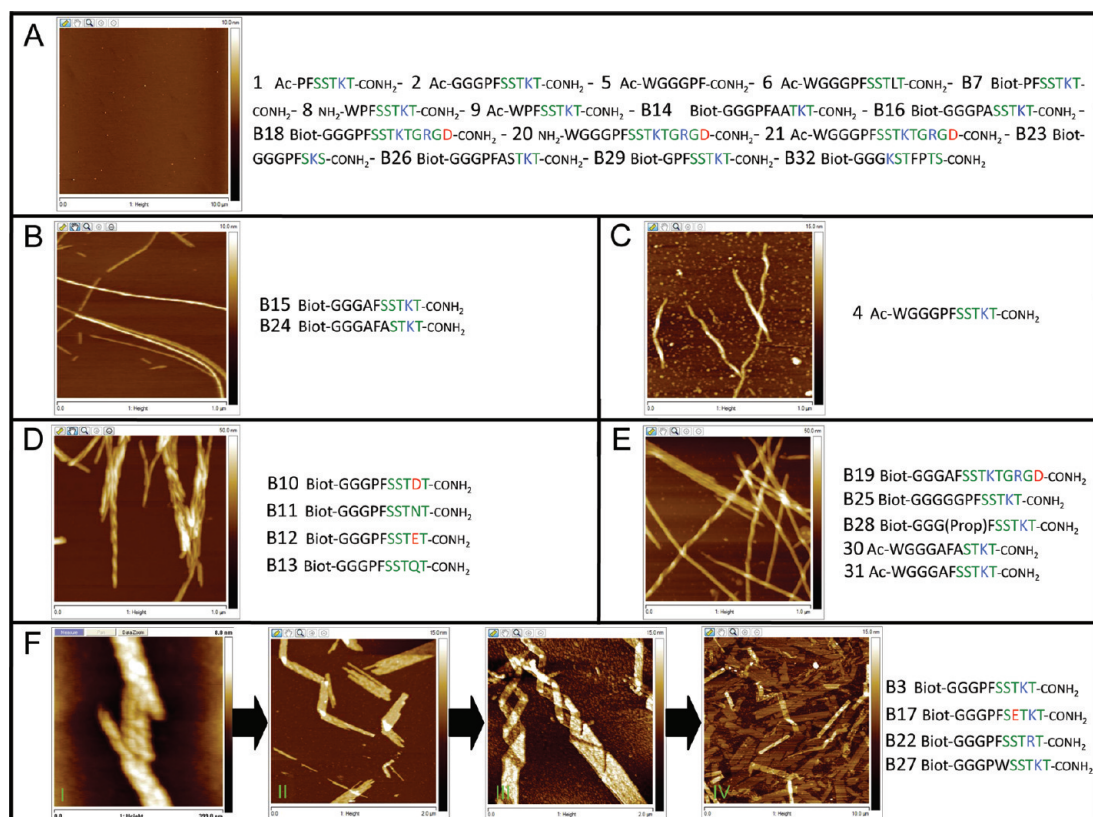
Figure 2. AFM imaging and classification of the tested BMHP1-SAPs. (A) Peptides that did not assemble at the macroscale did not shown any nanofibrous structure. (B) B15 and B24 self-assembled into flat tabular fibers. (C) Peptide 4 yielded twisted fibers. (D) Substitution of Lysine with a neutral or negatively charged residue gave immediately self-assembling peptides: indeed only chunks of assembled twisted fibers could be imaged. (E) Twisted fibers with different features were seen for peptide B19, B25, B28, 30, and 31 (see main text for details). B3, B17, B22, and B27 hierarchically self-assembled into twisted protofibrils (Fi), packed together to give ribbons (Fii), that assembled into straight tubular structures (Fiii) and eventually rearranged into flat sheets (Fiv). Black fonts stand for hydrophobic residues, green for polar ones, blue and red for positively and negatively charged residues, respectively.

was shown to be crucial for the self-assembling propensity of the chosen sequences: indeed when linked at the N-terminus it gave self-assembling peptides (B3 compared to peptide 2), and, when substituted with tryptophan, peptide solutions yielded lower G' values (peptides 4 and 30 compared to B3 and B24, respectively) and slower rate of the viscosity increments. Peptide functionalization with the polar RGD motif also prevented scaffold formation (B18, 20, and 21) or decreased the overall scaffold stiffness and increased the minimum necessary peptide concentration for gelation (B19) up to values like 3% (w/v). Lastly, the addition of the negatively charged Glu in B17 interfered with scaffold formation and decreased the overall G' of the assembled matrix (if compared to B3).

In summary, BMHP1-SAPs begin the self-assembling process upon dissolution in water. Storage moduli of peptide solutions increases along with peptide concentration and with time (Figure 1C), presumably an effect of their aggregation kinetics. Interestingly, G' value differences measured before and after PBS addition spanned some orders of magnitude (Supporting Information, Table S1) depending on the peptide sequence.

Others reported the increase in the hydrogel scaffold stiffness of β-hairpin peptides upon exposure to NaCl[31] as a consequence of the intermolecular folding triggered by the addition of salt ions. Indeed they demonstrated that self-assembly is frustrated by the electrostatic repulsion of the lysine residues, while the presence of salt ions screens electrostatic repulsions and allows for intermolecular hydrophobic interactions and H-bond formation, increasing the junction points of the fibrillary network and, as consequence, increasing the overall scaffold stiffness. Indeed Hartgerink and colleagues[32] showed how Lys-containing SAPs can produce interconnected fibrillary nanostructures by means of phosphate cross-linkings between lysine amines. However, we believe that the increases of G' moduli after PBS addition may more likely arise from interactions between overlapping nanofibers with screened surface charge[33] or from an increase in nanostructure fiber length.[34]

Morphological Characterization. AFM analysis of peptides not forming any hydrogel scaffold (see Table 1) showed no fibrous structure formation at the nano- and microscales (Figure 2A): identical results were obtained at various peptide concentrations (from

0.5% to 10% (w/v) concentrations) and up to one month after dissolution. On the contrary, BMHP1-SAPs formed various nanostructures that could be grouped in five categories as represented in Figure 2.

Pro-free peptides B15 and B24 self-organized into tabular long fibers (length ranging from 5 to 10 μm). Nanofiber heights were 1.6 ± 0.2 nm or fewfold bigger, while widths were 8.45 ± 0.49 nm or fewfold bigger, ascribable to fibers clamped together laterally (Figure 2B). Average fiber dimensions did not change significantly up to 10 days after dissolution.

Peptide 4 assembled into thicker and left-handed twisted fibers (minimum width of 30 nm) (Figure 2C), showing a pitch ranging from 100 to 150 nm (top-to-top horizontal distance). Heights, measured at the slope bottoms, were of 2.5 nm or fewfold bigger, spanning 5 nm (top-to-bottom vertical distance) within each twisted fiber. Notably, at day 1, 3, and 10 the density of imaged fibers increased over time, consistently with the observed slow viscosity increments of this BMHP1-SAP. Similarly, B19, B25, B28, 30, and 31 (Figure 2E) self-assembled into twisted left-handed fibers (average width of 15 and 30 nm; minimum heights were 6 and 12 nm) showing a vertical span of 6 nm between tops and bottoms of the twisted fibers (2 nm in the case of 30). Pitches ranged between 80 and 110 nm, except for B28 (from 30 to 40 nm). In the first days after dissolution they formed flat (peptide B19) and twisted (peptide 31) intermediate-fibers that eventually wrapped together giving similar twisted structures. Others reported the importance of the aromatic interactions in Phe–Phe peptides for tubular structure formation[35] or the supramolecular aggregate structure dependence on Pro–Phe relative positions,[36] thus suggesting Pro, Phe, and (in peptides 4, 30 and 31) Trp likely contribute to BMHP1-SAPs self-organization *via* hydrophobic and aromatic interactions. Noteworthy, peptide backbone linearization by substituting Pro with Ala made the difference between peptides not forming any scaffolds (B18, B26) and BMHP1-SAPs (B19, B24). On the other side, *N*-propylglycine substitution of Pro (B28) decreased G' and increased the minimum necessary peptide concentration for gelation up to 3% w/v (see Supporting Information, Table S1).

B10, B11, B12, and B13 self-assembled upon dissolution, giving scattered chunks of aggregated left-handed twisted fibers (Figure 2D). The rapid self-assembly, as a result of the neutral or negative total net charge, caused filaments to bundle together, reducing their potential for making solid scaffolds.

Lastly, peptides B3, B17, B22, and B27 self-organized into intermediate left-handed twisted protofibrils (Figure 2FI; width 8.5 nm or fewfold bigger; height 2–2.8 nm; pitches 28–30 nm for B3 and B22, 90–110 nm for B17 and B27) aligned side-by-side (day 1 after dissolution) and hierarchically aggregated in bigger ribbon-like long structures (featuring highly variable pitches and structures longer than 12 um) (Figure 2FII). These aggregates, both left- and right-handed, helically coiled (at day 3 postdissolution) to form straight tubular structures (Figure 2FIII) and eventually double- or multilayered sheets (at day 10) (Figure 2FIV), giving structures as high as 3–3.6 nm (2FIII) and 6.4 or 14 nm (2FIV), respectively. The presence of single-handed protofibrils (Figure 2FI) has been shown in other self-assembling peptides[37,38] and usually explained by the intrinsic chirality of the constituent peptide sequences. Differently, at a higher level of organization, multiple stable conformations are possible, thus not univocally imposing a unique orientation of the twisted ribbons (Figure 2FIII). Particularly, in this last set of BMHP1-SAPs the slow kinetics of the hierarchically self-assembly was clearly detectable up to 10 days, when growing microstructures, as big as several squared micrometers, were detected. BMHP1-SAPs in the group of Figure 2F, sharing the generic sequence biot-GGG-$PX_aSX_hX_hX_pX_h$, (X_a = aromatic residue; X_h = H-bond forming residues; X_p = positively charged residue), self-assemble at multiple levels of arrangements hierarchically. However, the insertion of longer Gly tails or the linking of a polar motif (RGD in B19) inhibit self-coiling of ribbons into tubular structures and sheets, supporting the importance of steric hindrance of the chosen BMHP1-SAP sequences allowing for higher levels of self-organization. Peptides were also imaged 1 h after dilution in PBS (1×) at 1 day after dissolution in water (see Experimental Methods for details). PBS caused BMHP1-SAP already formed nanostructures to randomly aggregate (Supporting Information, Figure S2) while no assembled structures were detected for peptides grouped in Figure 2A. Pitch and size of the clumped nanostructures were not altered by buffer addition while kinetic of formation of microscaled structures for peptides in Figure 2F was reduced, but not prevented, for weeks after dilution in PBS.

Characterization of Assembled Secondary Structures. Fibers of B3, 4, B12, B13, B15, and B19 were analyzed by X-ray diffraction (XRD) (see Experimental Methods for details) and gave isotropic rings with the maximum intensity at approximately 4.7 Å distance, usually ascribed to the H-bonding spacing between β-strands, typical of unaligned β-sheet forming fibers (Figure 3A).[39] Radial integration of the patterns revealed other diffraction peaks (Figure 3B) shared by all peptides, at 3.7–3.8 Å, typical van der Waals distance of packed peptide side-chains,[40] and 2.3–2.4 Å, considered as the second order of the 4.7 Å peak. Nonetheless these maxima gave a much less intense signal if compared to the 4.7 Å peak (Supporting Information, Table S2). Another clearly visible ring was found at 3–1.7 nm distance interval, yielding a medium intensity peak at 21 Å (arrow in Figure 3A) for peptides B3, B12, B13, at 2.86 and 2.35 nm for B19 and 4, respectively, and at 1.73 nm for B15. Peaks of distances greater than 1.5 nm were consistent with nanofiber heights measured
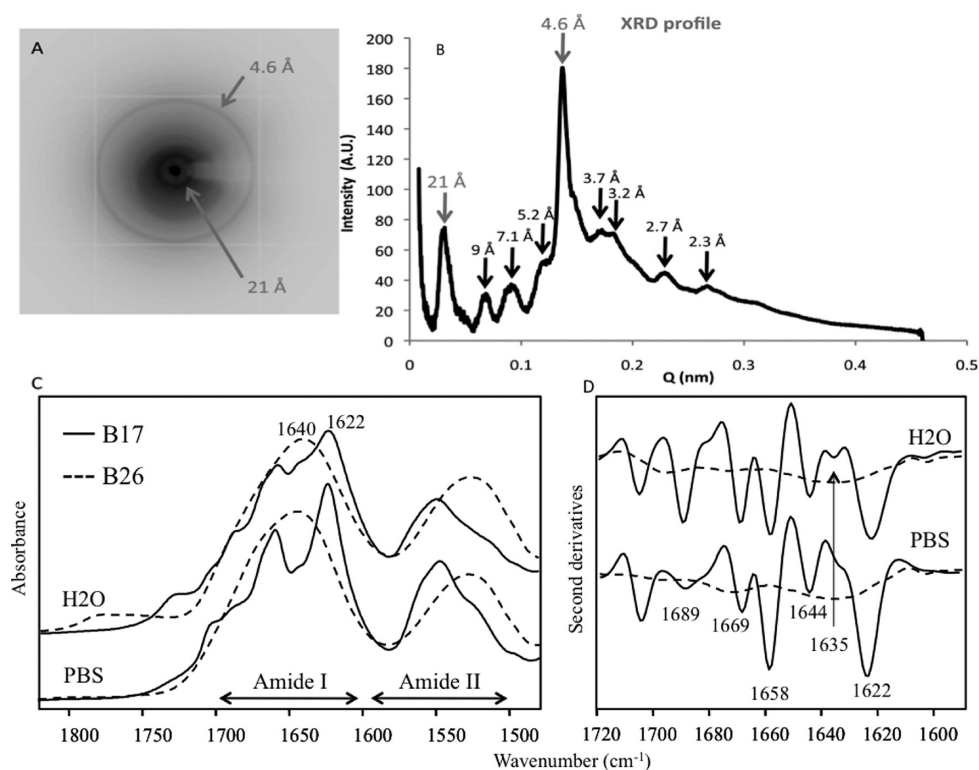
Figure 3. Structural characterization of BMHP1-SAPs. X-ray diffraction pattern (A) and radial integrated diffracted intensity (B) recorded for B3. Most significant peaks are identified at 21 and 4.6 Å, indicating the self-assembled fiber thickness and a predominant β-sheet secondary structure, respectively. The peak at 5.2 Å can be ascribed as distance between stacked aromatic groups. The 3.7 Å peak can be interpreted as chains packing at VDW distance. (C) ATR/FTIR spectra in the Amide I and Amide II absorption regions of B17 and B26, incubated for 24 h at a concentration of 3% (w/v). For comparison, the spectra of B17 and B26 are also reported after dilution in PBS at the final concentration of 1.5% (w/v). B26 was characterized by a random coil structure as suggested by its broad Amide I band centered at 1640 cm^{-1}, while the B17 spectrum, peaked at 1622 cm^{-1}, displayed several components that are better resolved in the second derivative spectra (D). The second derivative spectrum of B26 confirms a random coil structure, while that one of B17 displays two β-sheet components at 1635 and at 1622 cm^{-1} and several additional peaks with the following assignment: 1644 cm^{-1} due to hydrated open loop; 1658 cm^{-1} to random coil; 1669 cm^{-1} to β-turns; 1689 cm^{-1} to β-sheets and/or β-turns.

via AFM. Lastly, peaks between 5 and 8 Å, interpreted as intermolecular aromatic—aromatic interactions,[41,42] are more likely related to biotin interactions as they are not seen in the case of Trp substitution of biotin (peptide 4).

The presence of β-structures (both β-turns and β-sheets) in all BMHP1-SAP solutions at 1 day after dissolution was confirmed by circular dichroism in both water and PBS solutions (see Supporting Information, Figure S3).

Attenuated total reflection (ATR) FTIR experiments (Figure 3C,D) further confirmed and provided new insight in respect to the CD data. Indeed, FTIR spectroscopy allows one to monitor the formation of β-sheet structures in protein assemblies through the analysis of the Amide I band (from 1700 to 1600 cm^{-1}), due to the C=O stretching absorption of the peptide amide bond.[43] In Figure 3C we reported the spectra of B26 and B17, incubated for 24 h at a concentration of 3% (w/v), chosen respectively as examples of nonassembling peptides and BMHP1-SAPs. B26 displayed a broad Amide I band centered around 1640 cm^{-1} (Figure 3C), similarly to what observed in the spectra of other nonassembling peptides, that is, B7, B16, B29

(Supporting Information, Figure S4), whose absorption occurs in the range 1650—1640 cm^{-1}. This response indicates that a random coil secondary structure characterizes the nonassembling peptides.[43] This assignment was confirmed by the absorption spectrum of B26 measured in heavy water, as reported and discussed in Supporting Information, Figure S5. On the contrary, the Amide I band of B17 (Figure 3C), as well as of the other BMHP1-SAPs (Supporting Information, Figure S4), displayed several components in the measured absorption spectra. In the second derivative spectra,[44] these Amide I components appear as well-resolved peaks (Figure 3D and Supporting Information, Figure S4). Two components in the spectral region of the β-sheet structure absorption were observed for B17 at 1635 and at 1622 cm^{-1} that can be due to loosely and tightly packed β-sheet structures, respectively.[43,45] While the 1622 cm^{-1} peak can be assigned to intermolecular β-sheet structures in peptide assemblies, we cannot exclude that the 1635 cm^{-1} component, usually assigned to intramolecular β-sheet structures, might reflect a weaker intermolecular interaction. These assignments were confirmed by absorption spectra in heavy water

of B17 (Supporting Information, Figure S4) and B26. Similarly to B17, the majority of the other BMHP1-SAPs displayed the two β-sheet components in the range 1638−1629 cm^{-1} and 1623−1611 cm^{-1} (Supporting Information, Figure S4).

In addition, several well-resolved components were present in the spectra of B17 (Figure 3D) and of the other BMHP1-SAPs (Supporting Information, Figure S4). Possible peak assignments are the following: 1650−1643 cm^{-1} for hydrated open loop;[46] 1662−1657 cm^{-1} for random coil in peptide hydrated films;[47] 1671−1666 cm^{-1} for β-turns;[47] 1698−1684 cm^{-1} to β-sheet and/or β-turn structures.[47] Unexpectedly, these last components displayed in the second derivative spectra a very narrow band shape. This result suggests that not only β-sheets but also the above peptide structures are highly ordered in BMHP1-SAP.[43] We confirmed the presence of a high structural order in BMHP1-SAPs through the analysis of the NH stretching modes of the peptide bond in the range 3300−3100 cm^{-1} (Figure 4). In this spectral region, nonassembling peptides displayed a broad absorption, while BMHP1-SAPs were all characterized by an intense and very narrow band around 3273 cm^{-1}, which is indicative of an ordering of the NH amide groups.[43] To investigate the effects of PBS addition on nonassembling peptides and on BMHP1-SAPs, the samples were dissolved at a concentration of 3% (w/v) in distilled water, incubated at 4 °C for 24 h and then diluted in PBS at the final concentration of 1.5% (w/v) 1 h before ATR/FTIR measurements. The ATR/FTIR spectra clearly indicated that PBS addition induced only minor changes on the BMHP1-SAP secondary structures (Figure 3C,D, Supporting Information, Figures S6 and S7), suggesting that ion screening of charged residues allowed for more dense transient interactions, thus cross-linking the already formed nanostructures and yielding solid scaffolds.

Summarizing, β-sheet and β-turn packing were confirmed in all of the tested BMHP1-SAPs via XRD, CD, and FTIR experiments, indicating their similar secondary structure.

On the basis of these observations, we propose the two molecular models depicted in Figure 5 for BMHP1-SAPs. The FSSTKT "cores", propensive to β-structures[23] aggregation (stick representation), allow for the formation of β-sheet structures: in particular charged lysines likely favor the antiparallel conformation over the parallel one (preliminary molecular dynamic results not shown). When present, Pro truncates the β-sheet aggregation just before the Gly[48] and adds torsionality to formed β-structures yielding twisted protofibrils (Figure 5B). In the case of B15 and B24 nanofibers, given the presence of multiple heights, double or multiple layers may form (Figure 5A). We cannot exclude the formation of multiple bundles for the other Pro-containing BMHP1-SAPs. Trp aromatic residues or Biotins (green), when provided with considerable
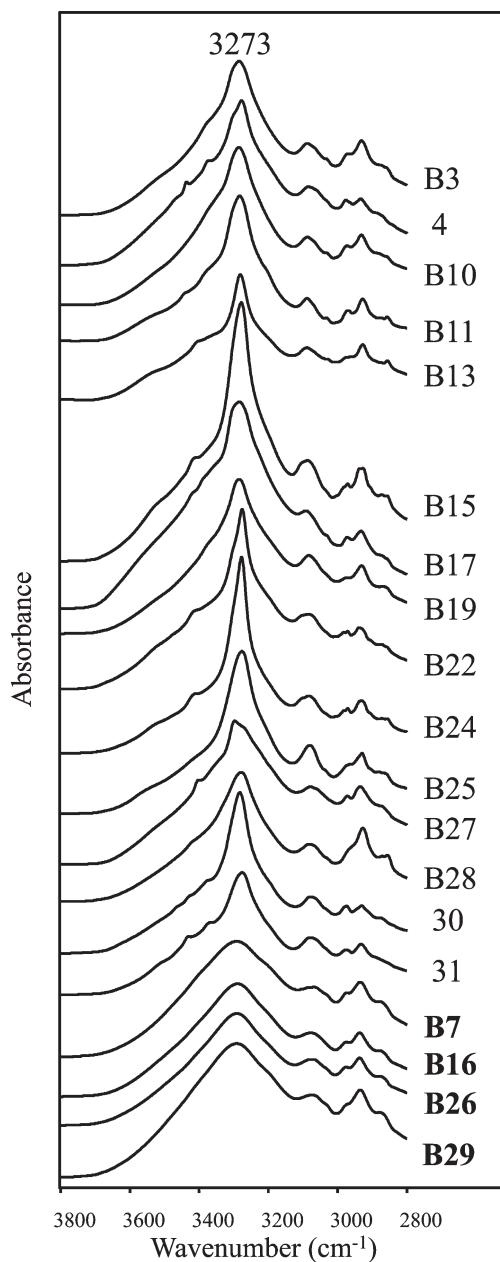

Figure 4. ATR/FTIR absorption spectra of the examined peptides in the region of the NH stretching vibration. Nonassembling peptides (B7, B16, B26, and B29) displayed a broad band in this region, while all the BMHP1-SAPs were characterized by a very narrow peak at ∼3273 cm^{-1}. This result indicates that BMHP1-SAPs formed highly ordered peptide assemblies. All spectra were reported after normalization to the Amide I band area.

degrees of freedom (spacer length > three residues) given by Gly (white), stabilize each aggregated subunit and act as zippers between tabular or twisted subunits by interacting with similar residues at the N-termini and/or with Pro, Phe, and Thr (right column, molecular surface representations).[26,27] The long Gly spacers also allow for intramolecular β-turn foldings of the tails (not shown in this model).

Zipper residues within twisted fibrils likely foster multiple levels of hierarchical self-aggregation along
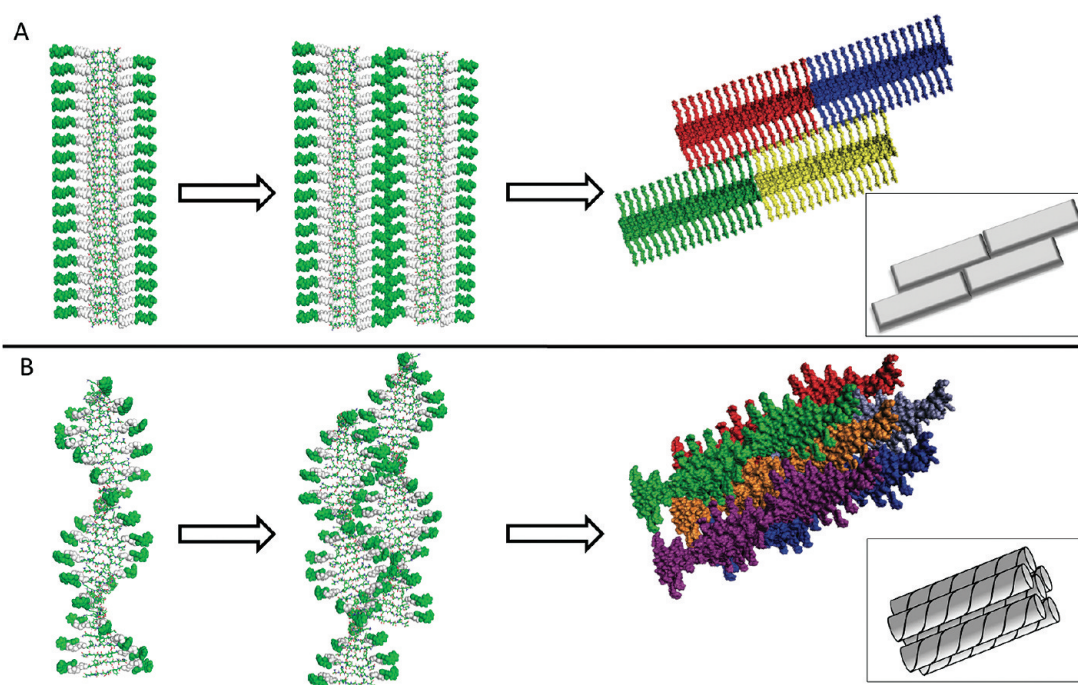
Figure 5. Proposed molecular model of assembly for B15 and B24 (A) and the other BMHP1-SAPs (B). In the first column residues involved in beta arrangements are drawn with sticks, while VDW representation is used for Gly (white) and biotin/Trp residues (green). The β-sheet inner cores are stabilized by aromatic-like interaction of the "tails", that, on their turn, can spontaneously fold into β-turns (not depicted here for sake of clarity). Double layers (A) or ribbons (B) are not depicted here but also possible. Pro exerts a left-handed twist over the β-sheet core giving helical structures (B), while Pro→Ala substitution allows for tabular fiber formation (A). Tails may also interact in a zip-like manner in both cases, allowing for laterally packed fibers (A) or fibrillary structures (B). Higher levels of possible self-aggregations are depicted to the right (molecular surface representations of different subunits have different colors) and schematized in the insets.

the three dimensions, as depicted in the inset of Figure 5B; however, further experiments have to be undertaken to clarify this hypothesis.

Self-Healing Hydrogels. BMHP1-SAPs were also verified for their self-healing propensity, namely, the capability of the assembled scaffolds to recover their stiffness in less than 12 h after a strain-induced rupture of the assembled gels. We measured the G' values of assembled scaffolds; samples were then subjected to rupture (strain sweep from 0.01% to 1000%). The G' values of samples were measured every 30 min *via* frequency sweep tests or, for long-term experiments, every 30 s *via* time sweep tests. For all BMHP1-SAPs, except for B19 and B28, G' values after rupture gradually increased, until full recovery, as depicted in Figure 6A, after which the G' values plateaued (Figure 6B). Additionally, multiple and consecutive mechanical breakages were obtained by stirring and vortexing the scaffolds previously assembled in transparent cuvettes (as seen in Figure 1A). Samples were checked for rupture by tilting. After a limited time (ranging from 1 to 12 h) the tested BMHP1-SAPs returned to their solidified gel appearance. This healing test could be successfully repeated at will. As found by others,[32] the different healing times shown by B17 (120′), B3 (6 h), B22 (11 h), B27 (90′) and other BMHP1-SAPs suggest that the recovery kinetics are strictly dependent on the peptide sequence.

Mechanical disruption of the assembled scaffolds acts at the macro- and mesoscale, sparing fragmentation on the smaller protofibrillary structures. BMHP1-SAPs feature a self-healing propensity at the mesoscale probably resulting from the rearrangement of the weak transient interactions spontaneously occurring between microscaled structures.

Scaffolds for *in Vitro* Cell Cultures and *in Vivo* Applications. To assess the potential of the BMHP1-SAPs for cell cultures and regenerative medicine, we cultured human neural stem cells (hNSCs) *in vitro*[11] over scaffolds made of B3, 4, B15, B17, B19, B22, B24, B25, B27, B28, 30, 31 (see Experimental Methods for details). Untreated tissue culture wells were chosen as negative control. At 7 days *in vitro* (DIV) we observed a heterogeneous degree of spreading of hNSCs over the various BMHP1-SAPs (see Figure 7A), ranging from proliferated cell clusters (in the case of B17), to bipolar cells (30), to adhered and branched hNSCs (B24). Other different extents of hNSC adhesion over BMHP1-SAP scaffolds are imaged in Supporting Information, Figure S8.

At 10 DIV live/dead cell fluorescence imaging showed a negligible number of dead cells (<3%) and confirmed the morphology evaluations drawn *via* light microscopy (data not shown). Indeed calcein-labeled living cells (Figure 7B) were imaged in round-shaped clusters (negative control), in poorly branched aggregates (B22) or were found distributed throughout the
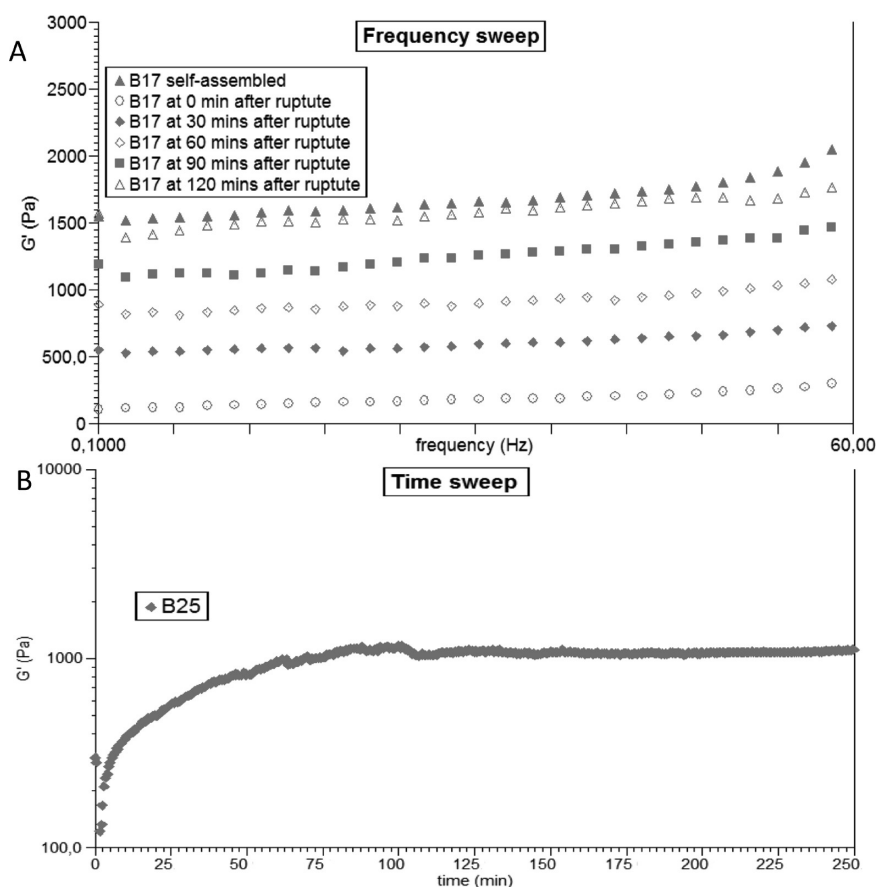
Figure 6. Self-healing tests. Frequency sweep (A) and time sweep (B) of the assembled scaffold after addition of PBS, after mechanical rupture, and at subsequent time points. In the case of B17 (A) the storage modulus recovered to values similar to those of the assembled scaffold before rupture in 120 min; in the case of B25 (B) G' values after rupture recovered in 100 min and steadily plateaued after recovery.

gel top-surfaces (low and high magnification pictures of B24).

CellTiter assay results, depicted in Figure 7C, showed that, except for peptides B25, BMHP1-SAPs significantly improved hNSC viability when compared to negative control ($P < 0.05$; paired t test). In particular, B24 showed the highest values of viable NSCs at 7 DIV, while in differentiation experiments at 14 DIV, the percentages of βIIITubulin+, MAP2+, GalC/O$_4$+, and GFAP+ cells (Figure 7D) were comparable to standard hNSC differentiation data obtained with animal extracts.[49]

The *in vitro* results demonstrate that BMHP1-SAPs fostered hNSC survival, spreading, and differentiation: promising qualities for 3D cell cultures and neural tissue engineering applications.[11] In most of the self-assembled scaffolds, the BMHP1 sequence, proved to stimulate hNSC proliferation and differentiation,[11] is either partially modified (B17, B25, B27, 30) or buried within the hierarchically aggregated structures (B3, B17, B22, and B27), impairing the exposure of whole active sequence for cell membrane receptor binding.[50] This is not the case for B24 and B15, where β-sheet tabular nanofibers allow a better solvent exposure of the functional motifs, giving a higher degree of hNSC

survival and adhesion. In particular B24 supported hNSCs differentiation toward neurons (βIIITubulin and MAP2 markers), astrocytes (GFAP marker), and oligodendrocytes (GalC/O$_4$ markers), the three main cell phenotypes of the central nervous system. To note, being that most of the G' values of BMHP1-SAP scaffolds are far above 100 Pa (besides 4, B19, and 30), we do not expect biomechanical properties to have played a significant role in hNSC viability assays.[51] Obtaining a hNSC differentiated progeny, *via* a synthetic injectable substrate, comparable to standard experiments conducted with natural positive controls, is a crucial starting point to develop functionalized scaffolds for regenerative *in vivo* applications.[11]

Indeed, the addition of the RGD motif (B19) can be considered as a proof-of-concept, giving results significantly different from negative control ($P < 0.002$: paired t test), that BMHP1-SAPs may be effectively functionalized. Other functional motifs may be adopted in the future by replacing RGD with more hydrophobic sequences like IKVAV.[21] In B28, where Pro was substituted with an *N*-propylglycine peptoid residue, giving more linearity to the molecule backbone and preserving the number of carbon atoms at the side chain without the characteristic
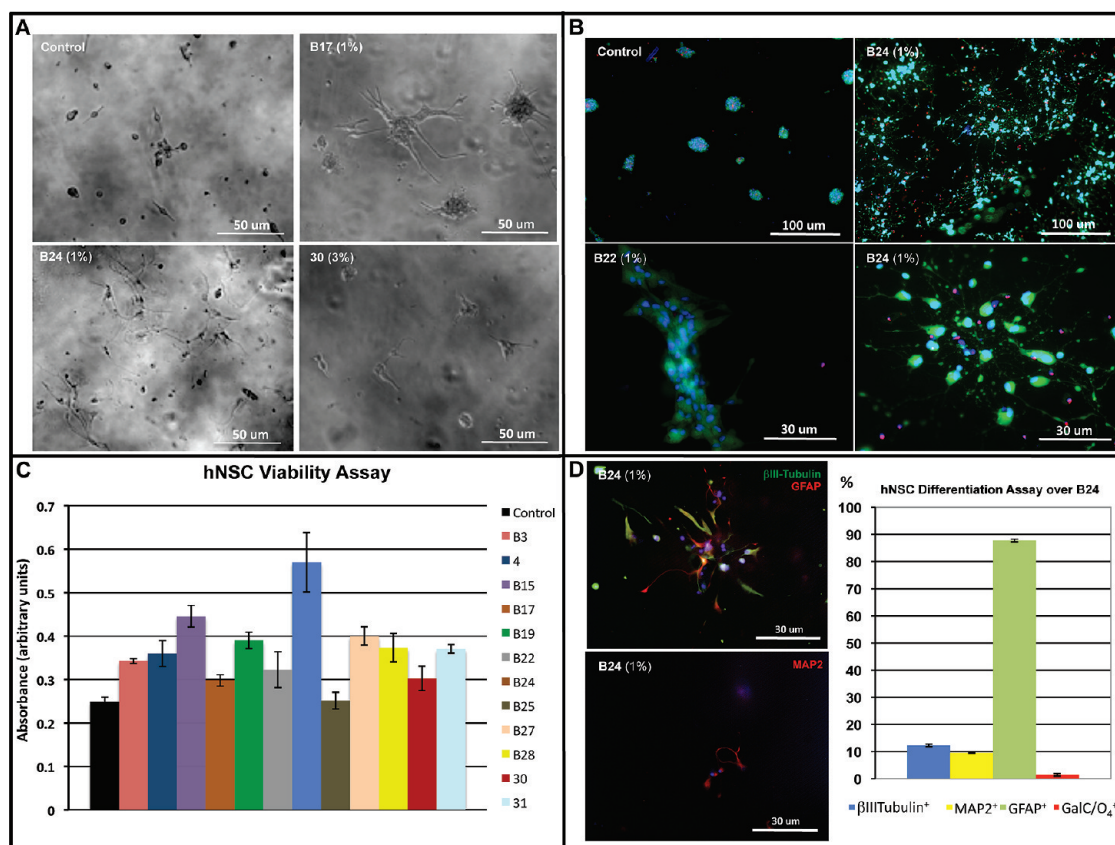
Figure 7. Human neural stem cells cultured over self-assembled scaffolds of BMHP1-SAPs. hNSCs were cultured for 7 DIV on self-assembled scaffolds of all BMHP1-SAPs. Among tested peptides, cell morphologies (A) comprised branched and adhered cells (B24), spreading clusters (B17), or poorly branched cells (30 and negative control). (B) Live/dead cell assays showed spherical clusters (negative control) of living cells (green), bipolar cells (B22), and layers of widely branched cells (B24). Dead cells/debris (a negligible amount was detected in all cases) are marked in red; cell nuclei are marked in blue. (C) Cell titer assay ($n = 6$) of cells cultured for 7 days over BMHP1-SAP scaffolds. B15 and B24 showed the biggest living cell populations, significantly different from negative control ($P < 0.002$ and $P < 0.001$, respectively; paired t test.). (D) NSCs cultured for 14 DIV over B24 scaffolds show positivity for GFAP (87.72% $\pm$ 0.49%), βIIITubulin (12.27% $\pm$ 0.49%), MAP2 (9.5% $\pm$ 0.1%) and GalC/O4 (1.63% $\pm$ 0.37%) markers ($n = 4$).
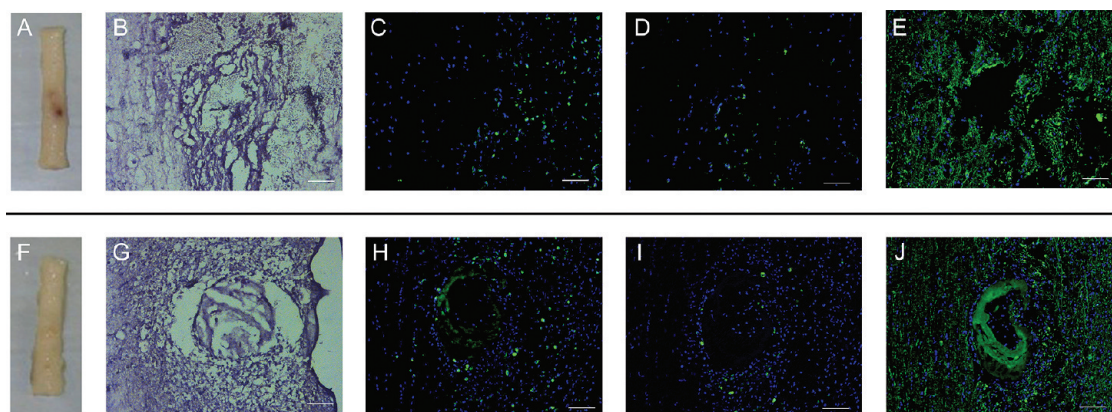

Figure 8. BMHP1-SAP biocompatibility *in vivo*. First row, animal belonging to control group; second row, treated animal. The hematoma spontaneously occurring in the spinal cord of saline-injected animals (A) was prevented in animals receiving injections of B24 (F). Hematoxilin-Eosin staining of the injection-site in saline-treated and in B24-treated animals (B and G, respectively). In control group and in treated animals we detected similar concentrations of infiltrated macrophages (green cells in C and H), apoptotic cells (green cells in D and I), and degenerating nervous fibers (green cells in E and J). Cell nuclei (blue) are stained with DAPI. Scale bar = 100 μm.

α-carbon of Pro, hNSC survival was comparable to those of the other peptides. This is another important result toward the design of new hybrid functionalized

sequences, made of peptides and peptoids, a class of peptidomimetics driving widespread interest,[52] amenable to easy functionalization with bioactive motifs at

their side-chains (*e.g.,* in the case of *S*-trityl-mercaptoethylamine). To test if any toxicity of these BMHP1-SAPs occurs when used *in vivo*, we assessed the tissue reaction to multiple injections of B24 into the spinal cord of rats (see Experimental Methods for details). Strikingly B24 prevented the hematoma physiologically forming after microinjections found in the control group (Figure 8F,G and 8A,B, respectively). Three days after injection, the spinal cord tissue of B24-injected animals displayed a negligible number of infiltrated macrophages and apoptotic cells in and around the area of the injections (Figure 8 panels H and I, respectively) if compared to saline-injected animals (Figure 8C,D). The neurofilament H dephosphorilated nervous fibers, considered as a symptom of degenerating nervous fibers,[53] were equally present in saline-injected and in B24-treated animals (Figure 8E,J). Summarizing, B24 prevented hematoma formation due to experimental surgery, it did not enhance either significant macrophages infiltration or apoptotic cell death and did not exacerbate nervous fibers degeneration when compared to saline-injected animals. Taken together these results give evidence for an appreciable short-term *in vivo* biocompatibility of the tested BMHP1-SAP.

CONCLUSIONS

We introduced and characterized a new ensemble of self-assembling peptides with (1) a recurrent presence of both β-sheets and β-turns in their secondary structures; (2) a concentration dependent kinetic of aggregation; (3) a hierarchical aggregation and self-healing propensity for some of the injectable hydrogels; and (4) a potential for *in vitro* cell cultures and *in vivo* applications. All of these are desirable properties for novel biomaterials in regenerative medicine.[54]

Among others, biotinylated BMHP1-SAPs offer a wide potential for applications in drug delivery and cell therapy,[55] both feasible approaches *via* modular functionalization of the assembled nanostructures with (strept)avidin-tagged cytokines or functional motifs. Alternatively, microtubular structures (B3, B17, B22, and B27) may be interesting carriers for drug delivery applications.[56] The described heterogeneous ensemble of characteristics at the nano- and microscales warrants multiple possible applications not limited to life-sciences for BMHP1-SAPs.[14] Lastly, further investigations and better understanding of the molecular arrangements of BMHP1-SAPs may increase the number of known strategies for the design of novel self-assembling materials.

EXPERIMENTAL METHODS

Peptide Synthesis and Purification. Peptides were synthesized on a 0.05 mmol scale with standard fluorenylmethoxycarbonyl solid-phase techniques using an AAPTEC peptide synthesizer. Rink amide resin (0.6 mmol/g substitution) was used to produce C-terminal amides; amino acids were dissolved in 0.4 M NMP with 0.4 M HoBt; 0.5 M Biotin with 0.4 M HoBt in DMSO solution was used for biotinylation. Peptides were then cleaved from the resin and deprotected with 4 mL of 95% trifluoroacetic acid (TFA), 2.5% water and 2.5% triisopropylsilane. Crude peptides were analyzed and purified by reverse phase HPLC using a Varian Galaxie system. Molecular weight of the peptides was confirmed with MALDI-TOF mass spectrometry (4800 Applied Biosystems). Final purity was more than 95%. For *in vitro* and *in vivo* experiments peptides were dissolved again in 50 mM HCl solutions and lyophilized to exchange TFA salts with HCl.

Rheological Tests. Rheological properties were determined using the controlled stress AR-2000ex rheometer (TA Instruments). A cone-and-plate geometry (acrylic cone diameter, 20 mm; angle, 1°; truncation gap, 34 μm) was used. All measurements were obtained at a temperature of 25 °C. Preliminary strain sweeps were performed for each sample to define the linear viscoelastic region. After adding approximately 10 volumes of PBS (1×, 154 mM ionic strength) laterally to the peptide solutions positioned in the 34 μm cone-and-plate gap of the rheometer as previously described,[30] time sweeps, were recorded at constant angular frequency (ω = 1 Hz). Frequency sweeps, both for peptide water solutions and for self-assembled scaffolds, were performed with the instrument in oscillatory mode at controlled strain of 1%. G' values were averaged in the 1−100 Hz region of n = 3 independent replicates. During self-healing tests the self-assembled scaffold was torn by applying a strain sweep (0.01%−1000% strain range) at 1 Hz oscillatory frequency: G' values were recorded in frequency sweep mode before and after the strain sweep step, measurements were performed every half hour. In the case of time sweeps performed for self-healing tests, values were recorded every half minute.

Atomic Force Microscopy. Peptides were dissolved in distilled water (GIBCO), at a concentration of 3% w/v one day prior imaging. Imaging and measurements were collected at day 1, 3, 7 and so on until a maximum observation time of 30 days. In the case of peptide scanned after buffer addition, peptides solutions were diluted with an equal volume of PBS (1×). Samples were then incubated for 1 h prior to next step. Right before imaging, peptides were diluted to 1% or 0.1% w/v; 2 μL of these solutions were placed on mica muscovite substrates and kept at room temperature for 2 min. The mica surfaces were then rinsed with distilled water, and solutions were let to evaporate for 30 min. AFM images were collected in tapping mode by a MultiMode Nanoscope IIIa (Digital Instruments) using single-beam silicon cantilever probes (Veeco RTESP: resonance frequency 300 kHz, nominal tip radius of curvature 10 nm, forces constant 40 N/m). Measurements were undertaken, *via* Veeco software, for approximately 100 different nanostructures detected in 6−8 fields per each peptide per each day of observation. The different nanostructures were grouped according to their dimensions and the numerosity of each group was considered as indicative of the most recurrent self-assembled structures. Values reported in the main text refer to the most recurrent structures (probability >75%).

When tabular nanofibers were detected and fiber height was between 1 and 1.5 nm, that is, far lower than the tip radius (10 nm), tip convolution effect was corrected with the formula[23,57]

$$\Delta x = \sqrt{2[h(2r_{\rm t} - h)]} \tag{1}$$

Where Δx is the width broadening effect, h is the nanofiber height, and $r_{\rm t}$ is the tip radius. Deconvolved results are expressed as means ± standard error of the mean ($n \geq 100$).

X-ray Diffraction Analysis (XRD). X-ray diffraction data were collected at a multiple-wavelength anomalous diffraction and monochromatic macromolecular crystallography beamline (5 T single pole superbend source with an energy range of 2.4−18 keV), at the Advanced Light Source located at Lawrence Berkeley National Laboratory. Data were collected with a 3 × 3 CCD array (ADSC Q315r) detector at a wavelength of 1.1159 Å. Data sets were collected at 200-mm distances with 40 s exposure times and 1° oscillations on a bulk sample of BMHP1-SAPs dissolved the day before at 3% w/v concentration. Peptide fiber solutions were centrifuged at 12 000 rpm for 10 min. The resulting concentrated solution was then dropped on a 0.2−0.3 mm diameter nylon loop and left to dry. Data were processed in Igor Pro 6.0 with a silver behenate (AgBE) standard.

Circular Dichroism. Far-UV CD spectra were recorded between 190 and 260 nm at room temperature on an Aviv 62DS spectrometer. All measurements were carried out in 1-mm quartz cuvette. Spectra were accumulated over 3 scans. CD spectra of peptide samples at 0.02%, 0.04%, and 0.06% w/v concentrations were collected at 1 day after dissolution (3% initial concentration) in water. Blank spectra of water were subtracted. Moreover PBS was added to the 3% peptide solutions bringing the peptide concentration to 1.5%, after 1 h samples were diluted at the concentrations previously described and scanned: in this case blank spectra of PBS were subtracted. Spectra were recorded in 2-nm steps, averaged over 4 s and normalized into Delta Epsilon units. Peptide structures were deconvolved *via* the CD Spectra Deconvolution Software 2.1 using 33 base-spectra of known proteins.

FTIR Analysis. Lyophilized peptides were dissolved at a concentration of 3% (w/v) in distilled water or D_2O (SIGMA), incubated at 4 °C for 24 h and then diluted at the final concentration of 1% (w/v) just before measurements. The spectra of all peptides were collected at both concentrations (1% and 3% w/v) in attenuated total reflection (ATR). A 1 μL portion of the peptide H_2O solutions was deposited on the nine reflection diamond element of the ATR device DuraSampl*IR* II (Smith Detection) and spectra were recorded after solvent evaporation to allow the formation of peptide hydrated films. The ATR/FTIR measurements were performed by the Varian 670-IR (Varian Australia Pty) spectrometer equipped with a nitrogen cooled mercury cadmium telluride detector and a dry air purging system. The following conditions were employed in the ATR/FTIR measurements: 2 cm^{-1} spectral resolution, 25 kHz scan speed, 512 scan coaddition, and triangular apodization. All the measured spectra were normalized to the Amide I band area and smoothed by a binomial function (11 points). The second derivatives were obtained by the Savitsky−Golay method (third grade polynomial, 5 smoothing points) using the GRAMS/32 software (Galactic Industries Corporation, Salem, NH, USA). In the case of peptides dissolved in D_2O, 10 μL of the peptide solution was deposited on the ATR element, and the infrared spectra were collected without evaporation of the solvent as described before. The peptide absorption spectra were corrected for the absorption of the D_2O solvent.

In Vitro Tests. Human NSCs were isolated and expanded as previously described.[49] The modalities for obtaining the primary tissue are in agreement with the guidelines of the European Network for Transplantation (NECTAR). Briefly, cells (at a concentration of 6 × 10^4 cells/cm^2) were seeded on the top-surface of each assembled scaffolds previously assembled into 96 multiwells. Negative control consisted of untreated bottom well surface. Initially, cells were cultured with basal medium supplemented with βFGF (10 ng/mL). At 3 days *in vitro* (DIV), βFGF medium was replaced with Leukemia Inhibitory Factor (LIF, Chemicon) (20 ng/mL) and Brain Derived Neurotrophic Factor (BDNF, Peprotech) (20 ng/mL). Fresh medium was added every 3 days.[11]

Live/dead cell imaging (Molecular Probes) at 10 DIV was obtained by following the manufacturer's protocol. At 7 DIV cell viability was quantified *via* CellTiter 96 Assay (Promega, Madison, WI) as recommended in the Promega protocol. After calibrating the linear response between the cell number and absorbance values, proliferated cell populations were quantified by using a Vmax microplate reader (Molecular Devices, Sunnyvale, CA) at

490 nm wavelength. Values, reported as means ± standard error of the mean, were blanked to their respective BMHP1-SAPs and cell culture media without cells. BMHP1-SAP results (n = 6) were assessed for their statistical significance in comparison with negative control *via* paired t tests.

To assess the differentiated phenotypes cells were stained at 14 DIV for βIIITubulin (Covance, 1:750), GFAP (Chemicon, 1:3000), MAP2 (Sigma, 1:200), GalC (Chemicon, 1:200), and O$_4$ (Chemicon, 1:200), subsequently marked with Cy3 (Jackson, 1:1000) and Alexa 488 (Molecular Probes, 1:1000) secondary antibodies. In details, cells were fixed in paraformaldehyde 4% for 15 min, permeabilized 10 min with PBS/0.1% Triton X-100, and blocked for 1 h with PBS/20% normal goat serum. Samples were incubated overnight in PBS/10% normal goat serum solutions of primary antibodies and incubated overnight at +4 °C. After several washes with PBS, secondary antibodies diluted in PBS/10% normal goat serum were applied for 1 h. Cell nuclei were counterstained with DAPI, samples were mounted with FluorSave reagent (Calbiochem), and samples were visualized and analyzed with Axiovert M200 fluorescence microscope. βIIITubulin$^+$, GFAP$^+$, GalC$^+$/O$_4$$^+$, and MAP2$^+$ cells were quantified by counting positive cells in four independent experiments.

In Vivo Experiments. All procedures involving animals were performed according to EC guidelines (EC Council Directive 86/609, 1987), to the Italian legislation on animal experimentation (Decreto L. vo 116/92) and to protocols approved by the Animal Care and Use Committee of the University of Milan-Bicocca (IACUC 37/07).

Female Sprague−Dawley rats weighting 200−250 g (Charles River Laboratories) were divided into two groups: (1) animals receiving injections of saline solution (control group, n = 3) and (2) animals treated with B24 (n = 3). Rats were anesthetized with an intraperitoneal injection of ketamine (80 mg/kg) and xylazine (10 mg/kg). The spinal cord was exposed at the T9-T10 level, and, after laminectomy, animals were injected with B24 (1% aqueous solution) or saline solution using a Hamilton syringe held *via* a micromanipulator. The solutions were delivered at distances of 500 μm, and two injections of 0.5 μL each were made at each interval, for a total dose of 3 μL. After injection, the muscles were sutured and the skin was closed with wound clips. Rats were treated daily with analgesic (carprofen, 5 mg/kg) and antibiotic (enrofloxacin, 5 mg/kg). Three days after surgery animals were sacrificed by transcardial perfusion with 4% paraformaldehyde. Spinal cords were removed, embedded in OCT, frozen, and sliced into 16 μm thick longitudinal sections. For immunofluorescence analysis slices were permeabilized and blocked with PBS/0,3% TritonX-100/10% normal goat serum (NGS) for 1 h at room temperature. Then slices were incubated 16 h with the following primary antibodies diluted in PBS/0.3% TritonX-100/1% NGS: Mouse Monoclonal CD68 (Serotec, 1:500) and Mouse Monoclonal SMI 32 (Covance, 1:1000). Goat anti Mouse Alexa 488 (Molecular Probes, 1:1000) secondary antibody diluted in PBS/0.3% TritonX-100/1% NGS was used for signal detection by incubating slices for 1 h. Cell nuclei were counterstained with DAPI (Roche), and slices were mounted with Fluorsave (Calbiochem). For histochemical analysis, slices were stained with hematoxylin/eosin. Tunel assay was performed using the *In Situ* Cell Death Detection Kit (Roche) according to the manufacturer's instructions. Images were taken with Zeiss Apotome Observer Z.1.

For each staining, analyses were performed on six contiguous slices of the injection sites per each animal.

Supporting Information Available: Tables S1−S2 and Figures S1−S8. This material is available free of charge *via* the Internet at http://pubs.acs.org.

REFERENCES AND NOTES

1. Tibbitt, M. W.; Anseth, K. S. Hydrogels as Extracellular Matrix Mimics for 3d Cell Culture. *Biotechnol. Bioeng.* **2009,** *103,* 655–663.

2. Hamidi, M.; Azadi, A.; Rafiei, P. Hydrogel Nanoparticles in Drug Delivery. *Adv. Drug Delivery Rev.* **2008,** *60,* 1638–1649.

3. Nisbet, D. R.; Crompton, K. E.; Horne, M. K.; Finkelstein, D. I.; Forsythe, J. S. Neural Tissue Engineering of the CNS Using Hydrogels. *J. Biomed. Mater. Res. B* **2008,** *87,* 251–263.

4. Anumolu, S. S.; Desantis, A. S.; Menjoge, A. R.; Hahn, R. A.; Beloni, J. A.; Gordon, M. K.; Sinko, P. J. Doxycycline Loaded Poly(ethylene glycol) Hydrogels for Healing Vesicant-Induced Ocular Wounds. *Biomaterials* **2010,** *31,* 964–974.

5. Negredo, E.; Puig, J.; Aldea, D.; Medina, M.; Estany, C.; Perez-Alvarez, N.; Rodriguez-Fumaz, C.; Munoz-Moreno, J. A.; Higueras, C.; Gonzalez-Mestre, V.; *et al.*Four-Year Safety with Polyacrylamide Hydrogel To Correct Antiretroviral-Related Facial Lipoatrophy. *AIDS Res. Hum. Retroviruses* **2009,** *25,* 451–455.

6. Bader, R. A.; Rochefort, W. E. Rheological Characterization of Photopolymerized Poly(vinyl alcohol) Hydrogels for Potential Use in Nucleus Pulposus Replacement. *J. Biomed. Mater. Res. A* **2008,** *86,* 494–501.

7. Bhattarai, N.; Gunn, J.; Zhang, M. Chitosan-Based Hydrogels for Controlled, Localized Drug Delivery. *Adv. Drug Delivery Rev.* **2010,** *62,* 83–99.

8. Ho, S. T.; Cool, S. M.; Hui, J. H.; Hutmacher, D. W. The Influence of Fibrin Based Hydrogels on the Chondrogenic Differentiation of Human Bone Marrow Stromal Cells. *Biomaterials* **2010,** *31,* 38–47.

9. Kleinman, H. K.; McGarvey, M. L.; Hassell, J. R.; Star, V. L.; Cannon, F. B.; Laurie, G. W.; Martin, G. R. Basement Membrane Complexes with Biological Activity. *Biochemistry* **1986,** *25,* 312–318.

10. Kisiday, J.; Jin, M.; Kurz, B.; Hung, H.; Semino, C.; Zhang, S.; Grodzinsky, A. J. Self-Assembling Peptide Hydrogel Fosters Chondrocyte Extracellular Matrix Production and Cell Division: Implications for Cartilage Tissue Repair. *Proc. Natl. Acad. Sci. U.S.A.* **2002,** *99,* 9996–10001.

11. Gelain, F.; Bottai, D.; Vescovi, A.; Zhang, S. Designer Self-Assembling Peptide Nanofiber Scaffolds for Adult Mouse Neural Stem Cell 3-Dimensional Cultures. *PLoS ONE* **2006,** *1,* e119.

12. Zhang, S.; Gelain, F.; Zhao, X. Designer Self-Assembling Peptide Nanofiber Scaffolds for 3d Tissue Cell Cultures. *Semin. Cancer Biol.* **2005,** *15,* 413–420.

13. Ellis-Behnke, R. G.; Liang, Y. X.; You, S. W.; Tay, D. K.; Zhang, S.; So, K. F.; Schneider, G. E. Nano Neuro Knitting: Peptide Nanofiber Scaffold for Brain Repair and Axon Regeneration with Functional Return of Vision. *Proc Natl Acad Sci U S A* **2006,** *103,* 5054–5059.

14. Rajagopal, K.; Schneider, J. P. Self-Assembling Peptides and Proteins for Nanotechnological Applications. *Curr Opin Struct Biol* **2004,** *14,* 480–486.

15. Zhang, S.; Holmes, T.; Lockshin, C.; Rich, A. Spontaneous Assembly of a Self-Complementary Oligopeptide To Form a Stable Macroscopic Membrane. *Proc. Natl. Acad. Sci. U.S.A.* **1993,** *90,* 3334–3338.

16. Gazit, E. Self-Assembled Peptide Nanostructures: The Design of Molecular Building Blocks and Their Technological Utilization. *Chem. Soc. Rev.* **2007,** *36,* 1263–1269.

17. Holmes, T. C.; de Lacalle, S.; Su, X.; Liu, G.; Rich, A.; Zhang, S. Extensive Neurite Outgrowth and Active Synapse Formation on Self-Assembling Peptide Scaffolds. *Proc. Natl. Acad. Sci. U.S.A.* **2000,** *97,* 6728–6733.

18. Gelain, F.; Unsworth, L. D.; Zhang, S. Slow and Sustained Release of Active Cytokines from Self-Assembling Peptide Scaffolds. *J. Controlled Release* **2010,** *145,* 231–239.

19. Ellis-Behnke, R. G.; Liang, Y. X.; Tay, D. K.; Kau, P. W.; Schneider, G. E.; Zhang, S.; Wu, W.; So, K. F. Nano Hemostat Solution: Immediate Hemostasis at the Nanoscale. *Nanomedicine* **2006,** *2,* 207–215.

20. Segers, V. F.; Lee, R. T. Local Delivery of Proteins and the Use of Self-Assembling Peptides. *Drug Discovery Today* **2007,** *12,* 561–568.

21. Silva, G. A.; Czeisler, C.; Niece, K. L.; Beniash, E.; Harrington, D. A.; Kessler, J. A.; Stupp, S. I. Selective Differentiation of Neural Progenitor Cells by High-Epitope Density Nanofibers. *Science* **2004,** *303,* 1352–1355.

22. Tysseling, V. M.; Sahni, V.; Pashuck, E. T.; Birch, D.; Hebert, A.; Czeisler, C.; Stupp, S. I.; Kessler, J. A. Self-Assembling Peptide Amphiphile Promotes Plasticity of Serotonergic Fibers Following Spinal Cord Injury. *J. Neurosci. Res.* **2010,** *88,* 3161–3170.

23. Taraballi, F.; Campione, M.; Sassella, A.; Vescovi, A.; Paleari, A.; Hwang, W.; Gelain, F. Effect of Functionalization on the Self-Assembling Propensity of Beta-Sheet Forming Peptides. *Soft Matter* **2009,** *5,* 660–668.

24. Jitrapakdee, S.; Wallace, J. C. The Biotin Enzyme Family: Conserved Structural Motifs and Domain Rearrangements. *Curr. Protein Pept. Sci.* **2003,** *4,* 217–229.

25. Lei, Y.; Li, H.; Zhang, R.; Han, S. Theoretical Study of Cooperativity in Biotin. *J. Phys. Chem. B* **2007,** *111,* 14370–14377.

26. Freitag, S.; Le Trong, I.; Klumb, L. A.; Chu, V.; Chilkoti, A.; Stayton, P. S.; Stenkamp, R. E. X-ray Crystallographic Studies of Streptavidin Mutants Binding to Biotin. *Biomol. Eng.* **1999,** *16,* 13–19.

27. Saggio, I.; Laufer, R. Biotin Binders Selected from a Random Peptide Library Expressed on Phage. *Biochem. J.* **1993,** *295,* 903.

28. Zhao, X.; Zhang, S. Molecular Designer Self-Assembling Peptides. *Chem. Soc. Rev.* **2006,** *35,* 1105–1110.

29. D'Souza, S. E.; Ginsberg, M. H.; Plow, E. F. Arginyl−Glycyl−Aspartic Acid (RGD): A Cell Adhesion Motif. *Trends Biochem. Sci.* **1991,** *16,* 246–250.

30. Genove, E.; Shen, C.; Zhang, S.; Semino, C. E. The Effect of Functionalized Self-Assembling Peptide Scaffolds on Human Aortic Endothelial Cell Function. *Biomaterials* **2005,** *26,* 3341–3351.

31. Schneider, J. P.; Pochan, D. J.; Ozbas, B.; Rajagopal, K.; Pakstis, L.; Kretsinger, J. Responsive Hydrogels from the Intramolecular Folding and Self-Assembly of a Designed Peptide. *J. Am. Chem. Soc.* **2002,** *124,* 15030–15037.

32. Aulisa, L.; Dong, H.; Hartgerink, J. D. Self-Assembly of Multidomain Peptides: Sequence Variation Allows Control over Cross-Linking and Viscoelasticity. *Biomacromolecules* **2009,** *10,* 2694–2698.

33. Castelletto, V.; Hamley, I. W.; Cenker, C.; Olsson, U. Influence of Salt on the Self-Assembly of Two Model Amyloid Heptapeptides. *J. Phys. Chem. B* **2010,** *114,* 8002–8008.

34. Veerman, C.; Sagis, L. M.; Heck, J.; van der Linden, E. Mesostructure of Fibrillar Bovine Serum Albumin Gels. *Int. J. Biol. Macromol.* **2003,** *31,* 139–146.

35. Reches, M.; Gazit, E. Casting Metal Nanowires within Discrete Self-Assembled Peptide Nanotubes. *Science* **2003,** *300,* 625–627.

36. Joshi, K. B.; Verma, S. Sequence Shuffle Controls Morphological Consequences in a Self-Assembling Tetrapeptide. *J. Pept. Sci.* **2008,** *14,* 118–126.

37. Aggeli, A.; Nyrkova, I. A.; Bell, M.; Harding, R.; Carrick, L.; McLeish, T. C.; Semenov, A. N.; Boden, N. Hierarchical Self-Assembly of Chiral Rodlike Molecules as a Model for Peptide β-Sheet Tapes, Ribbons, Fibrils, and Fibers. *Proc. Natl. Acad. Sci. U.S.A.* **2001,** *98,* 11857–11862.

38. Zhang, S.; Marini, D. M.; Hwang, W.; Santoso, S. Design of Nanostructured Biological Materials through Self-Assembly of Peptides and Proteins. *Curr. Opin. Chem. Biol.* **2002,** *6,* 865–871.

39. Sunde, M.; Serpell, L. C.; Bartlam, M.; Fraser, P. E.; Pepys, M. B.; Blake, C. C. Common Core Structure of Amyloid Fibrils by Synchrotron X-ray Diffraction. *J. Mol. Biol.* **1997,** *273,* 729–739.

40. Perutz, M. F.; Finch, J. T.; Berriman, J.; Lesk, A. Amyloid Fibers Are Water-Filled Nanotubes. *Proc. Natl. Acad. Sci. U.S.A.* **2002,** *99,* 5591–5595.

41. Burley, S. K.; Petsko, G. A. Aromatic−Aromatic Interaction: A Mechanism of Protein Structure Stabilization. *Science* **1985,** *229,* 23–28.

42. Gsponer, J.; Haberthur, U.; Caflisch, A. The Role of Side-Chain Interactions in the Early Steps of Aggregation: Molecular Dynamics Simulations of an Amyloid-Forming Peptide from the Yeast Prion Sup35. *Proc. Natl. Acad. Sci. U.S.A* **2003,** *100*, 5154–5159.

43. Barth, A. Infrared Spectroscopy of Proteins. *Biochim. Biophys. Acta* **2007,** *1767*, 1073–1101.

44. Susi, H.; Byler, D. M. Resolution-Enhanced Fourier Transform Infrared Spectroscopy of Enzymes. *Methods Enzymol.* **1986,** *130*, 290–311.

45. Natalello, A.; Prokorov, V. V.; Tagliavini, F.; Morbin, M.; Forloni, G.; Beeg, M.; Manzoni, C.; Colombo, L.; Gobbi, M.; Salmona, M.; *et al.* Conformational Plasticity of the Gerstmann−Straussler−Scheinker Disease Peptide as Indicated by Its Multiple Aggregation Pathways. *J. Mol. Biol.* **2008,** *381*, 1349–1361.

46. Fabian, H.; Naumann, D.; Misselwitz, R.; Ristau, O.; Gerlach, D.; Welfle, H. Secondary Structure of Streptokinase in Aqueous Solution: A Fourier Transform Infrared Spectroscopic Study. *Biochemistry* **1992,** *31*, 6532–6538.

47. Arrondo, J. L.; Goni, F. M. Structure and Dynamics of Membrane Proteins as Studied by Infrared Spectroscopy. *Prog. Biophys. Mol. Biol.* **1999,** *72*, 367–405.

48. Li, S. C.; Goto, N. K.; Williams, K. A.; Deber, C. M. α-Helical, but Not β-Sheet, Propensity of Proline Is Determined by Peptide Environment. *Proc. Natl. Acad. Sci. U.S.A.* **1996,** *93*, 6676–6681.

49. Vescovi, A. L.; Parati, E. A.; Gritti, A.; Poulin, P.; Ferrario, M.; Wanke, E.; Frolichsthal-Schoeller, P.; Cova, L.; Arcellana-Panlilio, M.; Colombo, A.; *et al.* Isolation and Cloning of Multipotential Stem Cells from the Embryonic Human CNS and Establishment of Transplantable Human Neural Stem Cell Lines by Epigenetic Stimulation. *Exp. Neurol.* **1999,** *156*, 71–83.

50. Taraballi, F.; Natalello, A.; Campione, M.; Villa, O.; Doglia, S. M.; Paleari, A.; Gelain, F. Glycine-Spacers Influence Functional Motifs Exposure and Self-Assembling Propensity of Functionalized Substrates Tailored for Neural Stem Cell Cultures. *Front Neuroeng.* **2010,** *3*, 1.

51. Saha, K.; Keung, A. J.; Irwin, E. F.; Li, Y.; Little, L.; Schaffer, D. V.; Healy, K. E. Substrate Modulus Directs Neural Stem Cell Behavior. *Biophys. J.* **2008,** *95*, 4426–4438.

52. Zuckermann, R. N.; Kodadek, T. Peptoids as Potential Therapeutics. *Curr. Opin. Mol. Therapy* **2009,** *11*, 299–307.

53. Trapp, B. D.; Peterson, J.; Ransohoff, R. M.; Rudick, R.; Mork, S.; Bo, L. Axonal Transection in the Lesions of Multiple Sclerosis. *N. Engl. J. Med.* **1998,** *338*, 278–285.

54. Pochan, D. J.; Schneider, J. P.; Kretsinger, J.; Ozbas, B.; Rajagopal, K.; Haines, L. Thermally Reversible Hydrogels *via* Intramolecular Folding and Consequent Self-Assembly of a *de Novo* Designed Peptide. *J. Am. Chem. Soc.* **2003,** *125*, 11802–11803.

55. Davis, M. E.; Hsieh, P. C.; Takahashi, T.; Song, Q.; Zhang, S.; Kamm, R. D.; Grodzinsky, A. J.; Anversa, P.; Lee, R. T. Local Myocardial Insulin-like Growth Factor 1 (Igf-1) Delivery with Biotinylated Peptide Nanofibers Improves Cell Therapy for Myocardial Infarction. *Proc. Natl. Acad. Sci. U.S.A.* **2006,** *103*, 8155–8160.

56. Sedman, V. L.; Adler-Abramovich, L.; Allen, S.; Gazit, E.; Tendler, S. J. Direct Observation of the Release of Phenylalanine from Diphenylalanine Nanotubes. *J. Am. Chem. Soc.* **2006,** *128*, 6903–6908.

57. Jun, S.; Hong, Y.; Imamura, H.; Ha, B. Y.; Bechhoefer, J.; Chen, P. Self-Assembly of the Ionic Peptide EAK16: The Effect of Charge Distributions on Self-Assembly. *Biophys. J.* **2004,** *87*, 1249–1259.